

1 **A strain-specific epitope of Enterovirus 71 identified by cryoEM of the complex with Fab from**
2 **neutralizing antibody**

3

4 **Running title: Strain-specific Epitope of EV71**

5

6 **Hyunwook Lee^{a*}, Javier O. Cifuentes^{a*}, Robert E. Ashley^a, James F. Conway^b, Alexander M.**
7 **Makhov^b, Yoshio Tano^{c,d}, Hiroyuki Shimizu^c, Yorihiro Nishimura^{c,e}, Susan Hafenstein^{a#}**

8

9 *Shared first authorship

10 ^aDepartment of Medicine, The Pennsylvania State University College of Medicine, 500 University
11 Drive, Hershey, Pennsylvania 17033, USA

12 ^bDepartment of Structural Biology, University of Pittsburgh School of Medicine, 3501 5th Ave,
13 Pittsburgh, Pennsylvania 15260, USA

14 ^cDepartment of Virology II, National Institute of Infectious Diseases, 4-7-1 Gakuen,
15 Musashimurayama-shi, Tokyo 208-0011, Japan

16 ^dJapan Poliomyelitis Research Institute, 5-34-4 Kumegawa-cho, Higashimurayama-shi, Tokyo 189-
17 0003, Japan

18 ^eDivision of Infectious Diseases, The Children's Hospital of Philadelphia, 3615 Civic
19 Center Blvd., Philadelphia, PA 19104, USA

20 Corresponding author :

21 Susan Hafenstein

22 Division of Infectious Diseases, MC H036

23 Department of Medicine, Penn State University College of Medicine

24 500 University Drive, Hershey PA 17033

25 Email: shafenstein@hmc.psu.edu

26

27 Author contributions: HL, JOC and SH designed research; HL and JOC performed research; REA, AMM, and

28 JFC collected EM data; YT, HS, and YN produced antibodies and performed and analyzed neutralization assays;

29 HL processed and analyzed data; HL and SH wrote the paper.

30

31

32 Word Count Abstract: 149

33 Word Count Manuscript: 3063

34

35

36

37 **ABSTRACT:**

38 Enterovirus 71 (EV71) is a picornavirus that causes outbreaks of hand foot and mouth disease
39 (HFMD) primarily in the Asia-Pacific area. Unlike coxsackievirus A16, which also causes HFMD,
40 EV71 induces severe neuropathology leading to high fatalities especially among children under the age
41 of 6 years. Currently, no established vaccines or treatments are available against EV71 infection. The
42 monoclonal antibody (MAb), MA28-7, neutralizes only specific strains of EV71 that have a conserved
43 glycine at amino acid, VP1-145, a surface exposed residue that maps to the five-fold vertex, and has
44 been implicated in receptor binding. The cryo-electron microscopy structure of a complex between
45 EV71 and the Fab fragment of MA28-7 shows that only one Fab occupies each five-fold vertex. A
46 positively-charged patch, which has also been implicated in receptor binding lies within the Fab
47 footprint. We identify the strain-specific epitope of EV71 and discuss the possible neutralization
48 mechanisms of the antibody.

49 **INTRODUCTION:**

50 Enterovirus 71 (EV71) infection causes outbreaks of hand, foot, and mouth disease (HFMD)
51 predominantly in the Asia-Pacific region (1, 2). Whereas most EV71 infections are self-limiting,
52 neurological and systemic complications can develop that range from aseptic meningitis to encephalitis
53 and acute flaccid paralysis. Infection can lead to lethal pulmonary edema and heart failure (2) with
54 mortality especially high in young children under the age of 6 (2, 3). As seasonal outbreaks of HFMD
55 are recurring around the world, development of a vaccine and antiviral therapies for EV71 has become
56 an urgent concern.

57 A member of the *Picornaviridae* family, EV71 has a non-enveloped, icosahedral capsid comprised
58 of 60 copies of each of four viral structural proteins (VP1-4) (4). Recent studies have solved the
59 structures for three strains of EV71 (MY104 (5), Fuyang (6), and 1095 (7)) demonstrating that EV71
60 has the general features of picornavirus capsids including the five-fold “mesa” and the depression
61 around the mesa called the “canyon” (5–8). Conserved residues VP1-242K and 244K form positively-
62 charged patches on the five-fold mesa (6), and this symmetry-related clustering of positive charges have
63 been suggested as a common mechanism for heparan sulfate binding in Enteroviruses (9).

64 Several cellular receptors for EV71 have been identified: Scavenger receptor B2 (SCARB2), P-
65 selectin glycoprotein ligand-1 (PSGL-1), and heparan sulfate (HS) (10–12). SCARB2, which is
66 expressed on a broad variety of cell types, likely binds into the virus canyon and induces the transition
67 of the virion that is required for uncoating (13–15). PSGL-1, which is expressed exclusively on
68 lymphocytes, binds only specific EV71 strains and supports viral replication in lymphocytes in a PSGL-
69 1-dependent manner (11). According to recent studies, PSGL-1 and HS bind the positively-charged
70 patches on the five-fold mesa of EV71 and provide initial attachment on the cell (12, 16, 17). We

71 recently found that the PSGL-1 binding phenotype of EV71 strains is regulated by a single residue,
72 VP1-145 that maps to the center of five-fold mesa (16).

73 Linear epitopes of EV71 have been characterized in several studies using synthetic peptides or
74 inactivated whole virus (18–21). The epitopes, which induce cross-neutralization activity, are located at
75 the rim of the canyon on VP1 and VP2, where SCARB-2 binds (18–20). Strain-specific neutralizing
76 antibodies that recognize conformational-dependent epitopes have been generated and classified (22);
77 however, the epitopes have not been mapped. Structural studies can identify and map the conformational
78 epitopes, and elucidate antibody neutralization mechanisms, which support effective vaccine
79 development. Here we have characterized the EV71 MAb MA28-7 as having strain-specific
80 neutralization activity. We used cryo-EM to solve the structure of EV71 complexed with the Fab from
81 MA28-7. The Fab binds across the five-fold symmetry axes such that steric hindrance limits occupation
82 to no more than one Fab per five-fold vertex. The footprint of the Fab includes VP1-145 and residues
83 that map to the positively-charged patches (VP1-98, 242, and 244) around the five-fold axis,
84 overlapping with the binding sites of PSGL-1 and HS. Neutralization and sequence alignment analysis
85 indicate VP1-145 is a determinant for the strain-specific antigenicity of EV71.

86

87 **MATERIALS AND METHODS:**

88 **Virus production:** EV71 was propagated and purified as described previously (8). Briefly, EV71
89 strain 1095 (23, 24) was propagated in HeLa cells for 24 hours. The media and cells were collected and
90 processed by freezing and thawing three times. Cell debris was pelleted by centrifugation and the
91 supernatant was precipitated with PEG 8K. After ultracentrifugation through a 30% sucrose-buffer
92 cushion, the pellets were re-suspended and applied to a 10-35% tartrate step-gradient. The virus was

93 collected and dialyzed against 10 mM Tris, 200 mM NaCl, 50 mM MgCl₂, pH 7.5, and concentrated to
94 1.0 mg/ml.

95 **MAb production:** Immunization of mice and preparation of hybridomas were performed at the
96 NIPPON BIO-TEST LABORATORIES Inc. (Tokyo, Japan). BALB/c mice were immunized with
97 formalin-inactivated EV71 strain 1095 (50 µg/mouse) three times every two weeks. Splenocytes were
98 isolated, and fused with myeloma cells, and hybridomas were generated. Antibodies from hybridoma
99 cell lines were screened for their ability to bind intact EV71 1095 virions and formalin-inactivated
100 virions in a sandwich enzyme-linked immunosorbent (ELISA) assay. The antibody used for these
101 studies, MA28-7, showed a weak binding activity to native virions of EV71 strains 1095, C7/Osaka and
102 SK-EV006, but did not bind to EV71 strains Nagoya, Bulgaria, and BrCr/tr or CA16 in the ELISA assay
103 (Tano Y, et al. unpublished data).

104 **Fab and virus-Fab complex preparation:** MAb of MA28-7 was obtained from ascite fluid after
105 inoculation of the hybridoma to BALB/c mice. The MAb was purified using HiTrap Protein G HP
106 columns (GE healthcare) according to the manufacturer's instructions. The MA28-7 Fab fragment
107 (Fab28-7) was generated by applying the MAb to papain immobilized-beads and purified by protein A
108 column (Pierce Fab Preparation Kit; Thermo Fisher Scientific). Initially purified virus and Fab were
109 incubated for 1 hour with a molar ratio of 1:240 (virus capsid:Fab), providing an excess of 4 Fabs per
110 each of the predicted 60 binding sites. Subsequently, a second incubation of 1:24 (virus capsid:Fab) was
111 done to allow 2 Fabs per each of the 12 possible binding sites of one per five-fold symmetry vertex to
112 reduce the protein background of unbound Fab for the asymmetric reconstruction.

113 **Cryo-EM imaging:** The two incubations were processed separately as data set 1 and 2,
114 corresponding to virus:fab ratios of 1:240 and 1:24, respectively (see above). For each, three µl of
115 virus:Fab complex were pipetted onto a Quantifoil grid (Quantifoil Micro Tools GmbH, Jena,Germany),

116 blotted to remove excess sample, and plunge-frozen into a liquid ethane/propane mixture (25) using a
117 Mk III Vitrobot (FEI, Hillsboro, Oregon). Low dose conditions were used to record images on Kodak
118 SO-163 film (Kodak, Rochester, New York) in an FEI TF-20 electron microscope operating at 200 KV
119 with calibrated magnifications of 30,000x and 50,000x for datasets 1 and 2, respectively. The
120 microscope was equipped with a Gatan 626 cryoholder (Gatan, Inc, Pleasanton, CA). Cryo-EM images
121 were collected with a defocus range of 2.73-4.16 μ m (dataset 1; Fig. 1A) and 1.9-6.12 μ m (dataset 2; Fig.
122 1B). Films were scanned using a Nikon Super Coolscan 9000 (Nikon, Melville, NY) giving a calibrated
123 pixel size at the sample of 2.12 \AA /pixel and 1.27 \AA /pixel for datasets 1 and 2, respectively. The program
124 suite AUTO3DEM (26) and EMAN2 (27) were used for image processing and 3D reconstructions.

125 **Icosahedral reconstruction of the complex:** Virus-Fab complexes from 16 micrographs of dataset
126 1 were used for calculating a three-dimensional reconstruction (Table 1). Semi-automatic particle
127 selection was performed using EMAN2's e2boxer.py to obtain the particle coordinates, followed by
128 particle extraction, linearization, normalization, and apodization of the images using Robem (26).
129 Defocus and astigmatism values to perform contrast transfer function (CTF) correction were assessed
130 using Robem for the extracted particles (Table 1). The icosahedrally-averaged reconstruction was
131 initiated using a random model generated from the raw data (26) and reached 10.5 \AA resolution
132 estimated where the Fourier Shell Correlation, FSC, dropped below 0.5. The absolute pixel size (2.08
133 \AA /pixel) and handedness were confirmed using UCSF Chimera (28) to compare the density map with
134 one calculated from the crystal structure of EV71 Fuyang strain (PDB ID : 3VBS).

135 **Asymmetric reconstruction:** Images of the virus-Fab complex of dataset 2 were selected with the
136 EMAN2's e2boxer.py. An icosahedrally-averaged reconstruction and assessment of absolute pixel size
137 (1.23 \AA /pixel) and handedness were performed as described above. The resulting 3D map was used as
138 an initial model for generating an asymmetric reconstruction with the following modifications: the Fab

139 density (radii >165 Å) of the 3D map was removed using AUTO3DEM's PCUT program and a small
140 sphere of density, 15 pixels in radius, was built on the capsid shell adjacent to one of the five-fold
141 symmetry axes using Robem (26). The modified map was rotated to the EMAN2 standard orientation
142 and the EMAN2 e2ctf.py module was used to manually determine the CTF parameters. The phases were
143 rectified for 6,539 images selected from 45 micrographs and the images were low-pass filtered at 10 Å
144 by e2proc2d.py. The 3D orientation of each particle was determined using standard refinement
145 procedures in EMAN2 with the 'breaksym=1' flag on the orientation generator to generate projections
146 for C1 symmetry. Each particle contributed to the five best scored classes by a 'sep=5' flag to generate a
147 smoother map and roughly 20% of the particles were discarded during the refinement process (27). The
148 resolution of the map was determined by e2eotest.py (Fig. 1C).

149 **Fitting of a Fab structure and roadmap of the Fab footprint:** Fitting of the atomic structure of
150 murine antibody Fab 3GK8 (29) was done first by eye and then refined in UCSF Chimera (28). The
151 refined fit of the Fab (correlation coefficient value of 0.743) was used to identify all atoms within 4 Å of
152 the fitted virus structures to generate the Fab-binding footprint. Stereographic projections were done
153 using the program RIVEM (30) and Coulombic representations of the surface were generated using
154 chimera (28).

155 **Neutralization assay:** The neutralizing titer of the EV71 antibodies was measured by following a
156 standard micro-neutralization assay. Briefly, in quadruplicate, the original ascitic fluid of BALB/c mice
157 was serially diluted in a 96-well tissue culture plate and each well mixed with an equal volume of EV71
158 (100 TCID₅₀ /50 µl). The plate was incubated at 36°C for 2 hours. After incubation, a cell suspension of
159 Vero cells (2×10⁴ cells/100µl) was added to each well and the mixtures were incubated at 36°C. CPE
160 was read under an inverted microscope for 10 days. The neutralizing titer was recorded as the highest

161 dilution of ascitic fluid, which protects 50% of the wells showing CPE, and expressed as the reciprocal
162 (Table 2). The end point of each neutralizing titer was calculated by the Kärber formula.

163

164 **RESULTS:**

165 **Cryo-EM reconstruction of Fab28-7 bound to EV71.** Fab fragments of MA28-7 were used to
166 make virus-fab complex for visualization by cryoEM. Initial experiments were aimed at saturating 60
167 potential binding sites on the capsid with bound Fab to produce a homogeneous population of virus-Fab
168 complexes. In the resulting cryoEM images, electron density protruded visibly from the capsid edges,
169 but only a few Fab appeared to be bound per capsid (Fig. 1A). In addition, the cryoEM images had a
170 strong background likely to be unbound Fab protein, raising the possibility that 60 binding sites on the
171 capsid were not occupied.

172 The 10.5 Å (Fig. 1C) icosahedrally-averaged 3D reconstruction revealed irregularly shaped and
173 weak density located above the exterior surface of the capsid at each five-fold vertex (Fig. 2A), in
174 accordance with a Fab occupancy of fewer than 60 per capsid. In cases where the Fab footprint overlaps
175 a five-fold icosahedral symmetry axis, steric hindrance combined with the imposition of icosahedral
176 symmetry results in the Fab density appearing as a bi-lobed turret (31, 32). In our reconstruction,
177 however, the density on each five-fold vertex was smaller than expected and disconnected from the
178 capsid (Fig. 2A and B). This lack of five-fold averaged Fab density is likely due to averaging occupied
179 epitopes with those that are empty. However, the disconnection between the capsid and Fab may be an
180 effect of the Fresnel fringe or incomplete correction of the CTF. Further tests indicated that the “loss” of
181 Fab density is resulted from the phase-flipping application for CTF correction (data not shown). An
182 additional icosahedrally-averaged reconstruction was done with full CTF deconvolution applied by
183 Wiener filter, which showed Fab connected to virus, but the distal Fab densities were greatly reduced in

184 strength compared to the strong capsid and RNA core densities (data not shown). This lack of Fab
185 density relative to that of the capsid suggests partial occupancy of less than one Fab per five-fold vertex.

186 **Asymmetric reconstruction.** For each of the icosahedrally-averaged reconstructions, the resulting
187 Fab electron density (Fig. 2) was not large enough to accommodate a model of a Fab molecule due to
188 the partial occupancy and 60-fold symmetry averaging. Consequently we calculated an asymmetric
189 reconstruction where Fab-labeled vertices were aligned with each other to maximize the Fab signal (27)
190 (EM database accession number EMD-27331). The starting model was an icosahedral capsid in which a
191 small sphere of density was positioned on one of the five-fold vertices, and each particle was oriented so
192 that a Fab-labeled vertex aligned to the sphere-occupied vertex. The resulting 23.4 Å (Fig. 1C)
193 asymmetric reconstruction had noticeable icosahedral features and a strong asymmetric density
194 corresponding to one Fab protruding from a single five-fold vertex (Fig. 3A). The volume of the Fab
195 density was about 3 times larger than the volume of the small sphere used in the starting model. There is
196 also weak density corresponding to Fab at the opposite vertex.

197 **Pseudo-atomic model and footprint of the Fab.** The X-ray crystal structures of EV71 MY104
198 strain (5) and Fuyang strain (6) were fitted separately into the asymmetric virus-Fab cryoEM
199 reconstruction by superimposing symmetry elements. The crystal structure of a murine antibody Fab
200 (3GK8)(29) was fitted into the Fab density to identify contacts on the virus surface (Fig. 3B) (PDB
201 accession code 3J3Z). All contacts within the Fab footprint mapped to VP1, with most residues located
202 on the BC- and HI-loops of two adjacent VP1 proteins. Six of the predicted contacts occur twice within
203 the Fab footprint (Fig. 4A and B), so that the effects of a single point mutation would be multiplied and
204 the effect on the footprint enhanced by the symmetrical five-fold environment. Residues of the five-fold
205 positively-charged patch (VP1-98K, 242K, 244K) (6) contribute significantly to the Fab footprint. The
206 two X-ray crystal structures have oppositely charged residues for VP1-98 (MY104:Glu and 3VBS:Lys),

207 which alters the electrostatic potential of the antibody binding site between the two strains (16) (Fig. 4C
208 and D). Within the antibody-binding footprint, the surface potential of the 1095 strain would more
209 closely resemble that of the MY104 strain.

210 **Strain-specific neutralization activity.** The neutralization activity of MA28-7 was tested against
211 six EV71 strains, including genotypes A, B1, B3, B4, and C2 (Table 2). EV71 strain C7/Osaka (B4),
212 SK-EV006 (B3), and 1095/Shiga (C2), were sensitive to neutralization by MA28-7, whereas strains
213 Nagoya (B1), Bulgaria (B1) and BrCr/tr (A) were resistant. The VP1 protein sequences of the six strains
214 were aligned to find any relationship between the antibody neutralization specificities (data not shown).
215 93.6% (278 out of 297) of amino acid residues were conserved among the six strains. Within the
216 antibody-binding footprint, only three residues varied in identity (Table 2). A glycine at VP1-145 is
217 conserved between neutralization-sensitive strains, whereas the strains that were resistant to antibody
218 neutralization have VP1-145E/A. In addition, neutralization-sensitive strains have VP1-98E and 242K,
219 whereas neutralization-resistant strains have VP1-98E/K and VP1-242K/E, suggesting that Glu98 and
220 Lys242 may be necessary, but not sufficient for antibody neutralization (16).

221

222 **DISCUSSION:**

223 **Low occupancy of Fab and asymmetric reconstruction.** The Fab binds across the five-fold
224 symmetry axis such that only one Fab can bind each vertex. Previously two cryo-EM studies solved
225 structures of virus-Fab complexes in which Fab binds the five-fold axes of cucumber mosaic virus
226 (CMV) and human rhinovirus serotype 2 (HRV2) (31, 32). In both studies, steric hindrance limited the
227 number of Fabs occupying each five-fold vertex to one or two, depending on how closely the Fab bound
228 to the symmetry axis. The density of Fab relative to capsid was 20% for CMV and 40% for HRV2,
229 which correlates to the one and two Fab molecules binding per each five-fold vertex, respectively. In our

230 study, we find a situation similar to the CMV-Fab study, however the averaged Fab28-7 density was
231 <10% that of the EV71 capsid, indicating that not all EV71 five-fold vertexes were occupied. This low
232 occupancy was confirmed by comparison to a simulated model in which we reduced the Fab density to
233 10% (data not shown). Possibly, Fab 28-7 binds with low affinity. Consequently, an asymmetric
234 reconstruction was necessary to improve the accuracy of the Fab-fitting. Similar approaches with
235 different reconstruction packages have been used previously to visualize successfully unique features of
236 icosahedral capsids (33–35). Using this approach, a single Fab was reconstructed bound to one of the
237 five-fold vertices, providing a better quality map for fitting a Fab structure and identifying the antigenic
238 epitope.

239 **Neutralization mechanisms.** The orientation of bound Fab relative to the capsid surface allows only
240 monovalent-attachment of the antibody, which could result in cross-linking of virions (Fig. 5).
241 Additionally, about half the residues within the footprint map to the positively-charged patches (Fig. 4),
242 which are necessary for PSGL-1 binding (16) and predicted to confer HS binding (12). This overlap of
243 binding sites suggests that the antibody might compete with receptors during initial attachment.

244 **VP1-145 as an EV71 antigenicity-controlling switch.** Our data shows that the conserved glycine at
245 VP1-145 located within the Fab buried surface (Fig. 4B), correlates with MA28-7 neutralization-
246 sensitivity (Table 2). The identity of amino acid 145 also confers the PSGL-1 binding phenotype by
247 regulating the configuration of electrostatic potential of the positively-charged patch (16). This same
248 mechanism may influence the MA28-7 binding; however, the specific identity at VP1-145 dictates Mab
249 neutralization (Table 2). Additionally, Chen et al. classified antibodies that neutralize VP1-145E strains
250 (PSGL-1-nonbinding) but not VP1-145G/Q strains (PSGL-1-binding phenotype) (Fig. 6) (16, 36). VP1-
251 145 has been found to be under positive selection (37, 38) and has been implicated as one of the possible
252 determinants of virulence in humans (39, 40) and adaptation in the mouse (41–43). It is likely that the

253 EV71 antigenicity, as well as receptor-binding phenotype, is altered with a single mutation at VP1-145,
254 which may confer an advantage to EV71 for effective host infection and transmission.

255 Here we have identified the strain-specific conformational epitope of an EV71 neutralizing antibody.
256 The antibody footprint maps to the five-fold vertex and encompasses the positively-charged patch and
257 residue VP1-145. Our data indicate that the identity of VP1-145 is a determinant of the MA28-7
258 neutralization-sensitivity. MA28-7 can cross-link virions and might inhibit initial attachment of EV71
259 virions to the cell surface. Our study gives insights into how EV71 can regulate strain-specific
260 antigenicity and provides meaningful information for the development of EV71 vaccines.

261

262 **Acknowledgements:** The work was supported by NIH K22 A179271 and Max Lang Junior Faculty
263 Research Scholar Award to SH. YN and HS were supported in part by grants-in-aid for Scientific
264 Research from the Ministry of Education, Culture, Sports, Science and Technology of Japan, and for
265 research on emerging and re-emerging infectious diseases from the Ministry of Health, Labour and
266 Welfare, Japan. We gratefully acknowledge the use of the Core Facility of the Penn State College of
267 Medicine. We thank Steven Ludtke for helpful scientific discussion.

268

269 **References**

- 270 1. **McMinn PC.** 2002. An overview of the evolution of enterovirus 71 and its clinical and public health
271 significance. *FEMS Microbiol Rev* **26**:91–107.
- 272 2. **Solomon T, Lewthwaite P, Perera D, Cardoso MJ, McMinn P, Ooi MH.** 2010. Virology,
273 epidemiology, pathogenesis, and control of enterovirus 71. *The Lancet infectious diseases* **10**:778–
274 790.
- 275 3. **Ooi MH, Wong SC, Lewthwaite P, Cardoso MJ, Solomon T.** 2010. Clinical features, diagnosis, and
276 management of enterovirus 71. *Lancet Neurol* **9**:1097–1105.

- 277 4. **Brown BA, Pallansch MA.** 1995. Complete nucleotide sequence of enterovirus 71 is distinct from
278 poliovirus. *Virus Res* **39**:195–205.
- 279 5. **Plevka P, Perera R, Cardosa J, Kuhn RJ, Rossmann MG.** 2012. Crystal Structure of Human
280 Enterovirus 71. *Science* **336**:1274–1274.
- 281 6. **Wang X, Peng W, Ren J, Hu Z, Xu J, Lou Z, Li X, Yin W, Shen X, Porta C, Walter TS, Evans G, Axford**
282 **D, Owen R, Rowlands DJ, Wang J, Stuart DI, Fry EE, Rao Z.** 2012. A sensor-adaptor mechanism for
283 enterovirus uncoating from structures of EV71. *Nat Struct Mol Biol* **19**:424–429.
- 284 7. **Cifuentes JO, Lee H, Yoder JD, Shingler KL, Carnegie MS, Yoder JL, Ashley RE, Makhov AM,**
285 **Conway JF, Hafenstein S.** 2013. The EV71 strain 1095 structures of procapsid and mature virion. *J*
286 *Virol.*
- 287 8. **Shingler KL, Yoder JL, Carnegie MS, Ashley RE, Makhov AM, Conway JF, Hafenstein S.** 2013. The
288 Enterovirus 71 A-particle Forms a Gateway to Allow Genome Release: A CryoEM Study of
289 Picornavirus Uncoating. *PLoS Pathogens* **9**:e1003240.
- 290 9. **McLeish NJ, Williams CH, Kaloudas D, Roivainen MM, Stanway G.** 2012. Symmetry-Related
291 Clustering of Positive Charges Is a Common Mechanism for Heparan Sulfate Binding in Enteroviruses.
292 *Journal of Virology* **86**:11163–11170.
- 293 10. **Yamayoshi S, Yamashita Y, Li J, Hanagata N, Minowa T, Takemura T, Koike S.** 2009. Scavenger
294 receptor B2 is a cellular receptor for enterovirus 71. *Nat Med* **15**:798–801.
- 295 11. **Nishimura Y, Shimojima M, Tano Y, Miyamura T, Wakita T, Shimizu H.** 2009. Human P-selectin
296 glycoprotein ligand-1 is a functional receptor for enterovirus 71. *Nat Med* **15**:794–797.
- 297 12. **Tan CW, Poh CL, Sam I-C, Chan YF.** 2013. Enterovirus 71 uses cell surface heparan sulfate
298 glycosaminoglycan as an attachment receptor. *J Virol* **87**:611–620.
- 299 13. **Yamayoshi S, Koike S.** 2011. Identification of a Human SCARB2 Region That Is Important for
300 Enterovirus 71 Binding and Infection. *Journal of Virology* **85**:4937–4946.

- 301 14. **Chen P, Song Z, Qi Y, Feng X, Xu N, Sun Y, Wu X, Yao X, Mao Q, Li X, Dong W, Wan X, Huang N,**
302 **Shen X, Liang Z, Li W.** 2012. Molecular Determinants of Enterovirus 71 Viral Entry: CLEFT AROUND
303 GLN-172 ON VP1 PROTEIN INTERACTS WITH VARIABLE REGION ON SCAVENGE RECEPTOR B 2.
304 Journal of Biological Chemistry **287**:6406–6420.
- 305 15. **Yamayoshi S, Iizuka S, Yamashita T, Minagawa H, Mizuta K, Okamoto M, Nishimura H, Sanjoh K,**
306 **Katsushima N, Itagaki T, Nagai Y, Fujii K, Koike S.** 2012. Human SCARB2-dependent infection by
307 coxsackievirus A7, A14, and A16 and enterovirus 71. J Virol **86**:5686–5696.
- 308 16. **Nishimura Y, Lee H, Hafenstein S, Kataoka C, Wakita T, Bergelson JM, Shimizu H.** 2013.
309 Enterovirus 71 Binding to PSGL-1 on Leukocytes: VP1-145 Acts as a Molecular Switch to Control
310 Receptor Interaction. PLoS Pathogens : in press.
- 311 17. **Yamayoshi S, Ohka S, Fujii K, Koike S.** 2013. Functional Comparison of SCARB2 and PSGL1 as
312 Receptors for Enterovirus 71. Journal of Virology **87**:3335–3347.
- 313 18. **Li X, Mao C, Ma S, Wang X, Sun Z, Yi Y, Guo M, Shen X, Sun L, Bi S.** 2009. Generation of neutralizing
314 monoclonal antibodies against Enterovirus 71 using synthetic peptides. Biochem Biophys Res
315 Commun **390**:1126–1128.
- 316 19. **Liu C-C, Chou A-H, Lien S-P, Lin H-Y, Liu S-J, Chang J-Y, Guo M-S, Chow Y-H, Yang W-S, Chang KH-**
317 **W, Sia C, Chong P.** 2011. Identification and characterization of a cross-neutralization epitope of
318 Enterovirus 71. Vaccine **29**:4362–4372.
- 319 20. **Lim XF, Jia Q, Khong WX, Yan B, Premanand B, Alonso S, Chow VTK, Kwang J.** 2012.
320 Characterization of an Isotype-Dependent Monoclonal Antibody against Linear Neutralizing Epitope
321 Effective for Prophylaxis of Enterovirus 71 Infection. PLoS ONE **7**:e29751.
- 322 21. **Gao F, Wang YP, Mao QY, Yao X, Liu S, Li FX, Zhu FC, Yang JY, Liang ZL, Lu FM, others.** 2012.
323 Enterovirus 71 viral capsid protein linear epitopes: Identification and characterization. Virology
324 Journal **9**:26.

- 325 22. **Chen Y, Li C, He D, Cheng T, Ge S, Shih JW-K, Zhao Q, Chen P-J, Zhang J, Xia N.** 2013. Antigenic
326 analysis of divergent genotypes human Enterovirus 71 viruses by a panel of neutralizing monoclonal
327 antibodies: Current genotyping of EV71 does not reflect their antigenicity. *Vaccine* **31**:425 – 430.
- 328 23. **Nagata N, Shimizu H, Ami Y, Tano Y, Harashima A, Suzaki Y, Sato Y, Miyamura T, Sata T, Iwasaki**
329 **T.** 2002. Pyramidal and extrapyramidal involvement in experimental infection of cynomolgus
330 monkeys with enterovirus 71. *J Med Virol* **67**:207–216.
- 331 24. **Shimizu H, Utama A, Onnimala N, Li C, Li-Bi Z, Yu-Jie M, Pongsuwanna Y, Miyamura T.** 2004.
332 Molecular epidemiology of enterovirus 71 infection in the Western Pacific Region. *Pediatr Int* **46**:231–
333 235.
- 334 25. **Tivol WF, Briegel A, Jensen GJ.** 2008. An improved cryogen for plunge freezing. *Microsc Microanal*
335 **14**:375–379.
- 336 26. **Yan X, Sinkovits RS, Baker TS.** 2007. AUTO3DEM—an automated and high throughput program for
337 image reconstruction of icosahedral particles. *Journal of Structural Biology* **157**:73–82.
- 338 27. **Tang G, Peng L, Baldwin PR, Mann DS, Jiang W, Rees I, Ludtke SJ.** 2007. EMAN2: an extensible
339 image processing suite for electron microscopy. *J Struct Biol* **157**:38–46.
- 340 28. **Pettersen EF, Goddard TD, Huang CC, Couch GS, Greenblatt DM, Meng EC, Ferrin TE.** 2004. UCSF
341 Chimera—A visualization system for exploratory research and analysis. *Journal of Computational*
342 *Chemistry* **25**:1605–1612.
- 343 29. **Hafenstein S, Bowman VD, Sun T, Nelson CDS, Palermo LM, Chipman PR, Battisti AJ, Parrish CR,**
344 **Rossmann MG.** 2009. Structural comparison of different antibodies interacting with parvovirus
345 capsids. *J Virol* **83**:5556–5566.
- 346 30. **Xiao C, Rossmann MG.** 2007. Interpretation of electron density with stereographic roadmap
347 projections. *Journal of Structural Biology* **158**:182–187.

- 348 31. **Bowman VD, Chase ES, Franz AWE, Chipman PR, Zhang X, Perry KL, Baker TS, Smith TJ.** 2002. An
349 antibody to the putative aphid recognition site on cucumber mosaic virus recognizes pentons but not
350 hexons. *Journal of virology* **76**:12250–12258.
- 351 32. **Hewat EA, Blaas D.** 2006. Nonneutralizing Human Rhinovirus Serotype 2-Specific Monoclonal
352 Antibody 2G2 Attaches to the Region That Undergoes the Most Dramatic Changes upon Release of the
353 Viral RNA. *Journal of Virology* **80**:12398–12401.
- 354 33. **Hafenstein S, Palermo LM, Kostyuchenko VA, Xiao C, Morais MC, Nelson CDS, Bowman VD,**
355 **Battisti AJ, Chipman PR, Parrish CR.** 2007. Asymmetric binding of transferrin receptor to
356 parvovirus capsids. *Proceedings of the National Academy of Sciences* **104**:6585–6589.
- 357 34. **Cherrier MV, Kostyuchenko VA, Xiao C, Bowman VD, Battisti AJ, Yan X, Chipman PR, Baker TS,**
358 **Van Etten JL, Rossmann MG.** 2009. An icosahedral algal virus has a complex unique vertex decorated
359 by a spike. *Proceedings of the National Academy of Sciences* **106**:11085–11089.
- 360 35. **Jiang W, Chang J, Jakana J, Weigele P, King J, Chiu W.** 2006. Structure of epsilon15 bacteriophage
361 reveals genome organization and DNA packaging/injection apparatus. *Nature* **439**:612–616.
- 362 36. **Chen Y, Li C, He D, Cheng T, Ge S, Shih JW-K, Zhao Q, Chen P-J, Zhang J, Xia N.** 2012. Antigenic
363 analysis of divergent genotypes human Enterovirus 71 viruses by a panel of neutralizing monoclonal
364 antibodies: Current genotyping of EV71 does not reflect their antigenicity. *Vaccine*.
- 365 37. **Tee KK, Lam TT-Y, Chan YF, Bible JM, Kamarulzaman A, Tong CYW, Takebe Y, Pybus OG.** 2010.
366 Evolutionary genetics of human enterovirus 71: origin, population dynamics, natural selection, and
367 seasonal periodicity of the VP1 gene. *J Virol* **84**:3339–3350.
- 368 38. **Chen X, Zhang Q, Li J, Cao W, Zhang J-X, Zhang L, Zhang W, Shao Z-J, Yan Y.** 2010. Analysis of
369 recombination and natural selection in human enterovirus 71. *Virology* **398**:251–261.
- 370 39. **Chang S-C, Li W-C, Chen G-W, Tsao K-C, Huang C-G, Huang Y-C, Chiu C-H, Kuo C-Y, Tsai K-N, Shih**
371 **S-R, Lin T-Y.** 2012. Genetic characterization of enterovirus 71 isolated from patients with severe
372 disease by comparative analysis of complete genomes. *J Med Virol* **84**:931–939.

- 373 40. **Li R, Zou Q, Chen L, Zhang H, Wang Y.** 2011. Molecular analysis of virulent determinants of
 374 enterovirus 71. *PloS one* **6**:e26237.
- 375 41. **Arita M, Ami Y, Wakita T, Shimizu H.** 2008. Cooperative effect of the attenuation determinants
 376 derived from poliovirus sabin 1 strain is essential for attenuation of enterovirus 71 in the NOD/SCID
 377 mouse infection model. *J Virol* **82**:1787–1797.
- 378 42. **Chua BH, Phuektes P, Sanders SA, Nicholls PK, McMinn PC.** 2008. The molecular basis of mouse
 379 adaptation by human enterovirus 71. *Journal of General Virology* **89**:1622–1632.
- 380 43. **Huang S-W, Wang Y-F, Yu C-K, Su I-J, Wang J-R.** 2012. Mutations in VP2 and VP1 capsid proteins
 381 increase infectivity and mouse lethality of enterovirus 71 by virus binding and RNA accumulation
 382 enhancement. *Virology* **422**:132–143.
- 383 44. **Rossmann MG, Palmenberg AC.** 1988. Conservation of the putative receptor attachment site in
 384 picornaviruses. *Virology* **164**:373–382.
- 385 45. **Larkin MA, Blackshields G, Brown NP, Chenna R, McGettigan PA, McWilliam H, Valentin F,**
 386 **Wallace IM, Wilm A, Lopez R, Thompson JD, Gibson TJ, Higgins DG.** 2007. Clustal W and Clustal X
 387 version 2.0. *Bioinformatics* **23**:2947–2948.
- 388
- 389

390 **FIGURE LEGENDS**391 **Figure 1. CryoEM micrographs of data and the resolution of reconstructions.** (A and B)

392 CryoEM datasets of Fab28-7 incubated in excess with EV71 in a ratio of 240:1 and 24:1 (Fab:capsid)
393 for the Dataset 1(A) and 2(B), respectively. Arrows indicate where fab can be seen bound to capsid. The
394 scale bar represents 50 nm. (C) Plot showing Fourier shell correlation (FSC) vs spatial frequency of the
395 icosahedrally-averaged reconstruction (Dataset 1; black line) and asymmetric reconstruction (Dataset 2;
396 red line). Resolution of the reconstructions is assessed where the FSC curve crosses below a correlation
397 value of 0.5.

398 **Figure 2 The 3D image reconstruction and central section of the map.** (A and B) Surface

399 rendered map and central section from the 10.5 Å icosahedrally-averaged reconstruction of EV71-Fab
400 complex. The averaged Fab density indicates that steric hindrance allows no more than one Fab to bind
401 per five-fold vertex. The surface rendered map is radially colored according to the key and displayed at a
402 contour level of 0.4 σ . Icosahedral symmetry axes are indicated in the central section.

403 **Figure 3. The asymmetric reconstruction and fitted Fab structure.** (A) An asymmetric approach

404 aimed at reconstructing one Fab bound to the capsid surface resulted in strong Fab density ~30% the
405 magnitude of the capsid density. Shown here displayed at 1.0 σ , the icosahedral features of the capsid
406 are easily discerned and the surface rendered map is radially colored using same key as Fig. 2. (B) The
407 refined fit of the Fab structure with heavy chain (grey) and light chain (yellow) shown in wire
408 demonstrates the fit of a single Fab onto one five-fold mesa, which identifies the interactions of the Fab
409 with two subunits of the virus capsid. The fitted virus crystal structure is shown colored in the
410 convention for picornavirus: VP1-blue, VP2-green, VP3-red, and VP4-yellow.

411 **Figure 4. Roadmaps of virus surface at the five-fold vertex.** (A-D) A five-fold view of a pentamer

412 of the EV71 (4AED) viral surface is shown as a stereographic projection where the polar angles θ and ϕ

413 represent latitude and longitude, respectively (30). The virus surface is represented as a quilt of amino
414 acids (44). The asymmetric unit is shown in black lines. (A) Residues are colored according to radius. A
415 section of radial density, 158-160 Å, corresponding to Fab bound adjacent to the viral capsid, is
416 projected onto the five-fold road map with a yellow contour of density greater than 0.8. (B) One Fab
417 footprint is shown with dark blue contacts in one protomer (light blue) and red contacts in the adjoining
418 protomer (pink). (C and D) The five-fold projections of MY104 strains (5) (4AED) and Fuyang (6)
419 (3VBU) are shown with Coulombic surface coloring and an outline of the Fab binding footprint to
420 illustrate the differences.

421 **Figure 5. Monovalent-interaction of the Fab.** Using the refined fitted Fab structure, all 60
422 symmetry-related capsid-bound Fabs were generated. The distances between the heavy chain C-terminus
423 of adjacent Fabs and between the centers of each Fab footprint, show that adjacent Fabs are too far apart
424 to allow bivalent binding. Heavy chain and light chain are shown in grey and yellow wire, respectively,
425 with virus protomers colored according to VP, with the picornavirus convention VP1, 2, and 3 as blue,
426 green, and red, respectively. The two-fold symmetry axis is indicated by the arrow.

427 **Figure 6. Sequence alignments of the seventeen EV71 virus strains used in Chen et al (22).**
428 Strains in the red box (antigenic type 1, 2.1 and 2.2) are neutralized by class IIb 12 MAbs, whereas
429 strains in blue box (antigenic type 2.3 and 2.4) are not neutralized by the same class. VP1-145 is the
430 only residue that is conserved among strains in the red box exclusively. Clustal W (45) was used to align
431 the VP1 sequence from 96-155 for 17 EV71 strains that are listed by genbank accession ID code. Each
432 dot (.) refers to conserved sequence and the single letter identifier is used for residue identity.

433

434

435

436

437

438 **Table 1. Image data for cryoEM reconstruction**

439

Parameter	Dataset 1	Dataset 2
Virus : Fab ratio	1:240	1:24
No. of micrographs	16	45
Defocus level range (μm)	2.73-4.16	1.90-6.12
No. of particles selected from micrographs	2,864	6,539
No. of particles used for reconstruction	2,807	6,277 (27,026)
Final resolution (\AA)	10.5	9.72 (23.4)

440

441 *Values in () are for asymmetric reconstruction.

442

443

444

445

446

447

448

449

450

451

452

453

454

455

456

457

458

459

460

461

462

463

464

465

466

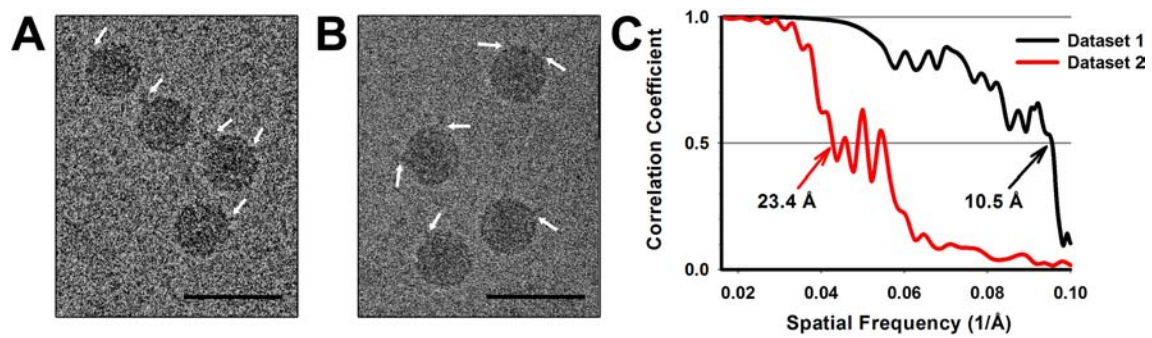
467
468
469
470
471
472

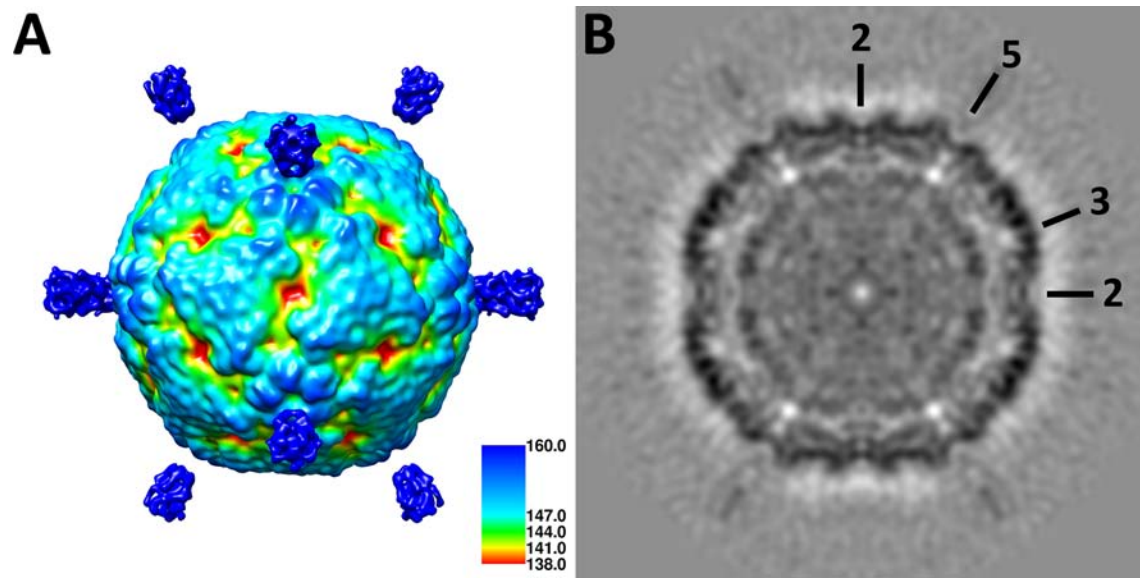
Table 2. Characterization of EV71 strains

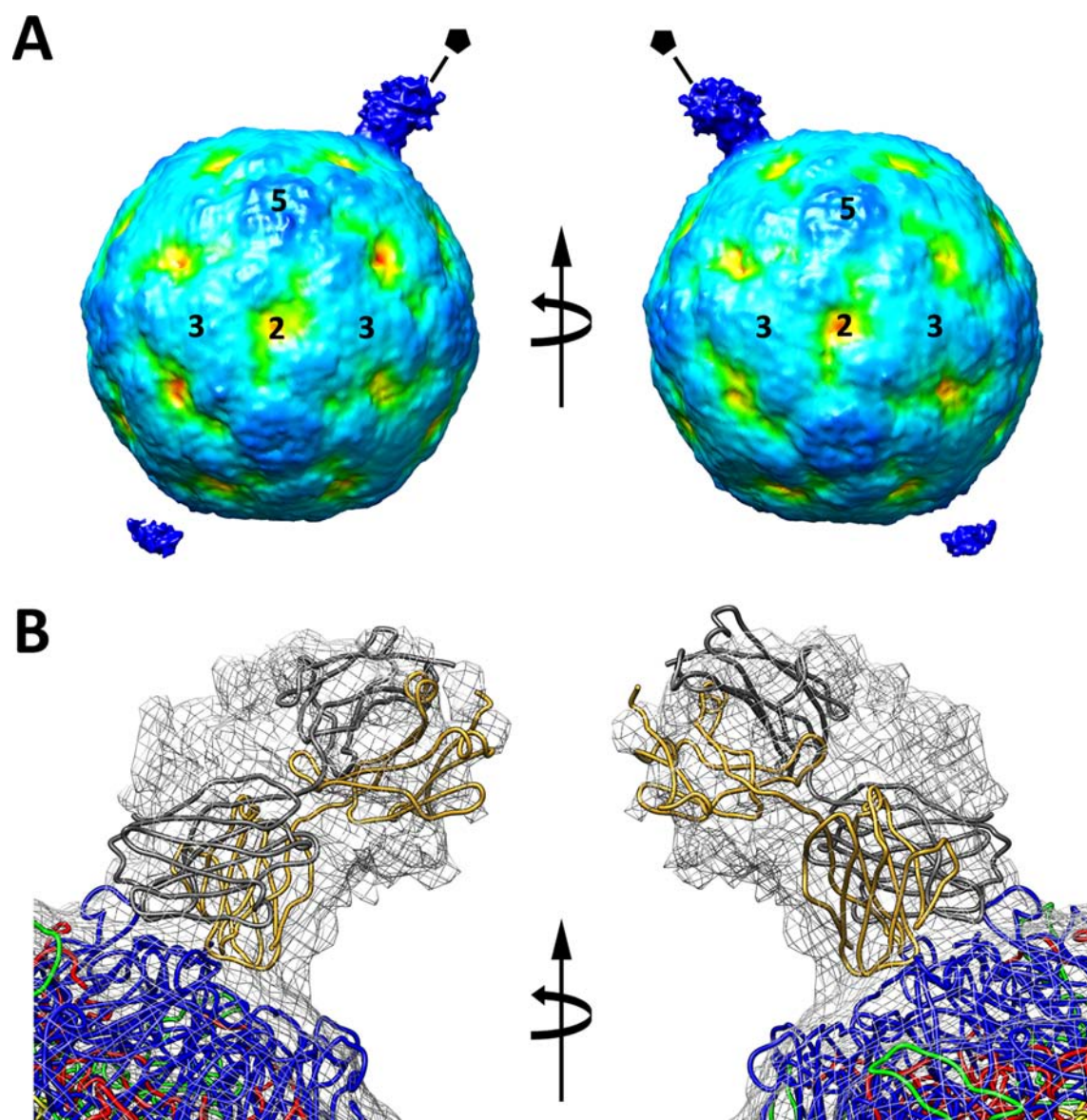
Strains	Genogroup	Neutralization titer	Amino acid residue				PSGL-1 binding
			98	145	241	242	
SK-EV006	B3	1350	Glu	Gly	Leu	Lys	PB
C7/Osaka	B4	1350	Glu	Gly	Leu	Lys	PB
1095/Shiga	C2	1130	Glu	Gly	Ser	Lys	PB
Bulgaria	B1	<200	Glu	Ala	Ser	Lys	*PB
BrCr/tr	A	<200	Lys	Glu	Ser	Gln	Non-PB
Nagoya	B1	<200	Glu	Glu	Ser	Lys	Non-PB

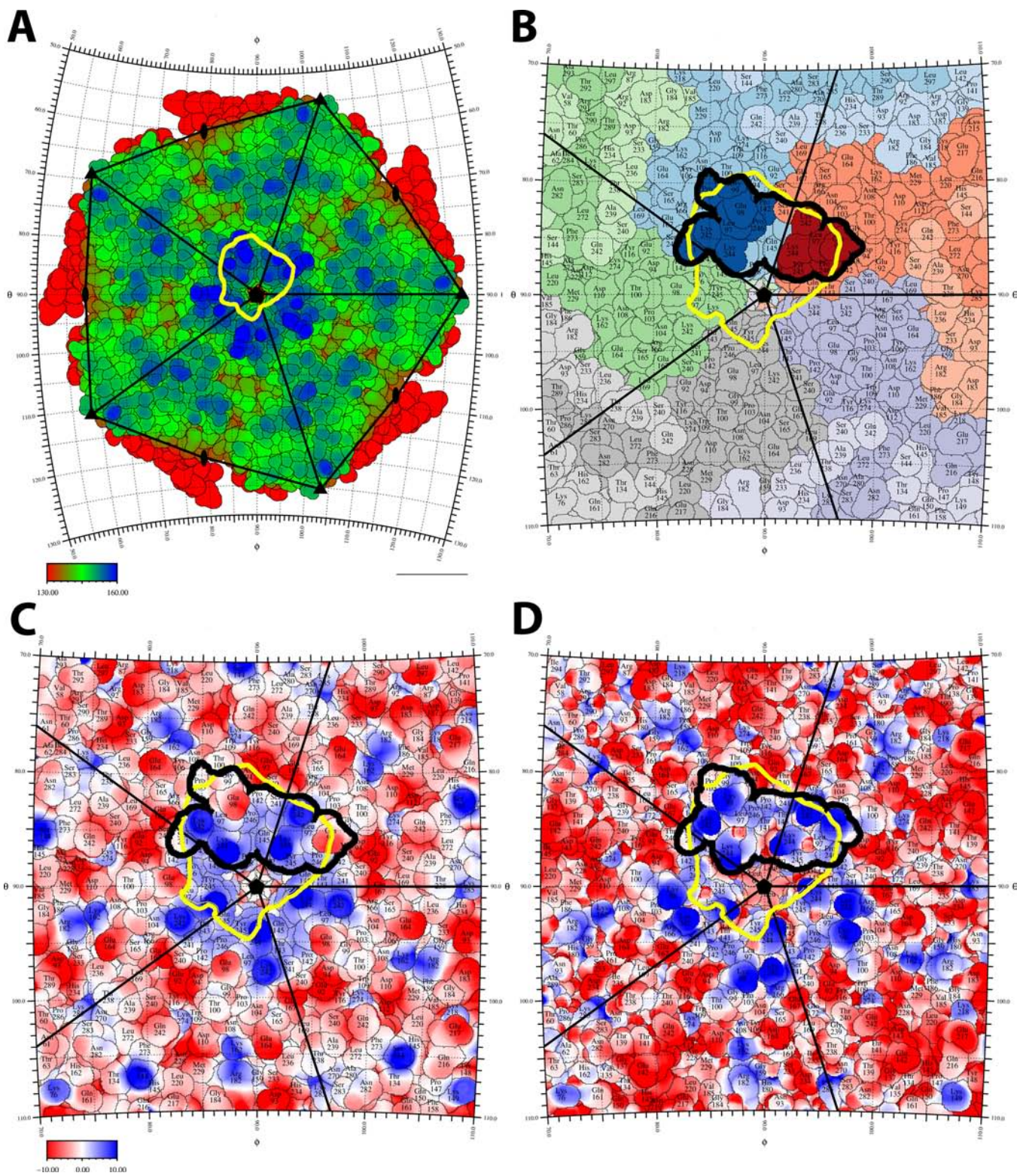
473
474 PB = PSGL-1-binding
475 Non-PB = PSGL-1-nonbinding
476 * a predicted phenotype based on (16).
477

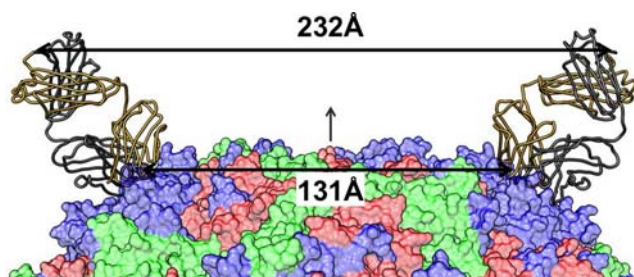
478
479
480
481
482
483
484











	96	145	155
FJ600325_Jiangsu	PLKGTTPNGYANWDIDITGYAQMRRKVELFTYMRFDAEFTFVACTPTGEVVPQLLQYMF		
JN646109_1985		
JQ042703_123		
JQ042705_3804	..E.....		
JF420578_H3	..E.....		
JF420579_H4		
JF420554_02969		
JF420552_03149	..E.....	..K.....	..K.....
JN964686_5535		
JN646108_NT22		
JQ042704_3803	..E.....		
JF420553_03315Q.....
JF420587_NT15	..E.....		..G.....
JF420580_H8	..E.....		..Q.....
AB469182_SK-EV006	..E.....		..G.....
JF420551_02205	..E.....		..Q.....
JF420549_02203	..E.....		..Q.....